Nanoscale

Accepted Manuscript

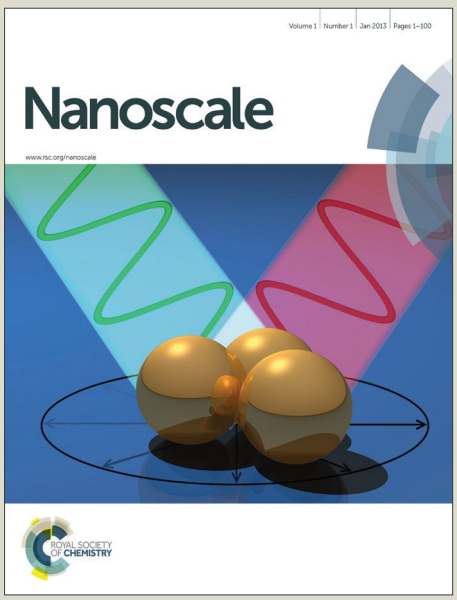

ROYAL SOCIETY OF CHEMISTRY

www.rsc.org/nanoscale

Cite this: DOI: 10.1039/c0xx00000x

www.rsc.org/xxxxxx

ARTICLE TYPE

Photoluminescent Carbon-Nitrogen Quantum Dots as Efficient Electrocatalyst for Oxygen Reduction

Jianhua Shen,[a] Yunfeng Li,[b] Yunhe Su,[a] Yihua Zhu,[a] Hongliang Jiang,[a] Xiaoling Yang,[a] Chunzhong Li[a]*

Received (in XXX, XXX) Xth XXXXXXXXX 20XX, Accepted Xth XXXXXXXXX 20XX
DOI: 10.1039/b000000x

Here, we demonstrate novel carbon-nitrogen quantum dots (CNQDs) by the hydrothermal method using melamine and glutaraldehyde. CNQDs are uniform dispersion with particle diameters of 3-8 nm. These prepared CNQDs show excellent luminescence properties and the photoluminescent quantum yields of CNQDs with 365 nm emission is up to 31 %. Interestingly, CNQDs possess the co-existence of both p- and n-type conductivities from the Mott-Schottky relationship. Furthermore, the electrochemical measurements reveal that CNQDs exhibit catalytic activity for the oxygen reduction reaction (ORR). However, the low electrical conductivity affect the ORR electrocatalytic activity. So the catalyst is conducted by chemical coupling CNQDs on Ag nanoparticles (NPs), the resulting CNQDs/Ag NPs catalyst is demonstrated to possess superior electrocatalytic ability for the ORR in an alkaline medium.

Introduction

Carbon nanomaterials, including fullerenes, carbon nanotubes, graphene, and mesoporous carbon, have attracted significant attention from the scientific community due to their unique properties and potential applications (adsorption, separation, catalysis, gas storage, and electrode materials, respectively).[1] More recently, photoluminescent (PL) carbon nanomaterials exhibit great potential for various optoelectronic applications due to their size/wavelength-dependent and edge-sensitive photoluminescence properties.[2] Compared to the semiconductor quantum dots and organic dyes, PL carbon quantum dots (CQDs) are superior in terms of chemical inertness, low photobleaching, no optical blinking, low cytotoxicity and excellent biocompatibility.[3] Therefore, advances in this area are appearing frequently, with a number of significant breakthrough applications, such as bioimaging, electrochemical biosensors and catalysis, and specifically in photovoltaic devices.[2] Although, many approaches have been developed to prepare CQDs, there is still a bottleneck for progress in controlling the size, morphology, and surface chemical composition of the products with high quantum yields (QYs > 30 %), which impede their applications in practice.[4] It has been demonstrated that functionalizing CQDs with nitrogen groups can enhance their properties and expand their other applications.[5,6] Despite several successes in the past reported, it is still of great urgency to develop simple and effective methods to synthesize nitrogen-doped PL CQDs with uniform morphology and high QYs.

Recently, there has been a trend to synthesize N-doped PL carbon nanomaterials for effectively tuning their intrinsic properties, including electronic characteristics, surface and local chemical features.[7] Interestingly, N-doped carbon nanomaterials (such as N-doped carbon nanotubes, N-doped graphene) showed high electrocatalytic activities for the oxygen reduction reaction (ORR).[8,9] Along with various methods developed for the preparation of N-doped PL carbon nanomaterials, Qu et al. used electrochemical process to create N-doped graphene quantum dots with a N/C atomic ratio of ca. 4.3 %, which showed luminescent and electrocatalytic activity.[9] Teng et al. synthesized N-doped graphene oxide quantum dots by calcination in NH_3 and reoxidation treatment, and the prepared photocatalysts (N/C ratio of only about 2.9 %) exhibited both p- and n-type characteristics.[10] However, these methods are relatively complex, and the atomic ratio of N/C is difficult to further increase, which might be conducive to further improve their fluorescence properties and catalytic activities.

Zhao et al. synthesized PL carbonaceous nanospheres with the nitrogen level as high as 11.36 atom% by hydrothermal treatment of cocoon silk.[1] Due to the surface passivation by various amine groups, the QYs was about 38 %. Herein, we present a simple hydrothermal treatment of melamine and glutaraldehyde to bottom-up synthesize water-soluble, high yield and PL carbon-nitrogen quantum dots (CNQDs), as shown in Fig. 1. The resultant CNQDs have a uniform morphology, with a size of ca. 5 nm, plentiful oxygen and nitrogen functional groups, and a high N/C atomic ratio of ca. 20.7 %. The obtained CNQDs show excellent and stable fluorescent properties with QYs of ca. 31 %. Moreover, CNQDs coupled with Ag nanoparticles (NPs), a new class of electrocatalysts for the ORR is obtained, which is alternative to the commercial Pt/C catalyst.

Experimental Section

Synthesis of CNQDs by hydrothermal method. Typically, 10 mL of melamine solution (8 mM in 0.1 M HCl) was thoroughly mixed into 15 mL of glutaraldehyde solution (8 mM) under vigorous stirring for 30 min. The mixture solution was then transferred into a 50 mL Teflon-lined stainless-steel autoclave and heated at 200 ^{o}C for 24 h. After cooling to room temperature,

the resulting solution was further dialyzed in a dialysis bag (retained molecular weight: 1,000 Da) a week and CNQDs were strong blue fluorescent, and the produce CNQDs yield is up to ca. 47 %. The prepared CNQDs were then dispersed in distilled water (ca. 6 mg mL^{-1}) for further characterization and uses.

Preparation of CNQDs/Ag NPs. The preformed Ag NPs were modified by the mercapto acetic acid. 0.5 mL of mercapto acetic acid was added into the above Ag NPs/ethanol solution and allowed to react for 3 h, yielding carboxylic acid modified Ag NPs. A certain amount of the as-prepared CNQDs (5 mL) was mixed with 0.3 mL carboxylic acid modified Ag NPs aqueous solution (0.02 g mL^{-1}) to form a homogeneous dispersion by slight ultrasonication. And then 1 mL of N-hydroxysuccinimide (NHS) and N-Ethyl-N'-[3-(dimethylamino)propyl] carbodiimide hydrochloride (EDC) (both of 0.1 mg mL^{-1}) were added quickly, followed by stirring for 2 h. The products were collected by centrifugation, washed with ethanol and distilled water several times, and finally dispersed in distilled water (ca. 6 mg mL^{-1}) for further uses.

Electrode preparation and electrochemical tests. The RDEs were polished with 1 and 0.05 μm alumina slurry sequentially and then washed ultrasonically in ultrapure water and ethanol, respectively. The catalysts (1 mL, 6 mg mL^{-1}) were ultrasonically dispersed in the mixed solution of Nafion (Nafion® 117 solution, ~5% in a mixture of lower aliphatic alcohols and water, 100 μL) and distilled water (900 μL), resulting in a catalyst concentration of 3 mg mL^{-1}. Then the catalyst dispersion (10 μL) was added dropwise onto the RDE, which yielded a loading of catalyst 0.15 mg cm^{-2}. The resulting electrode was dried under ambient conditions over night. Commercial 20 % Pt/C catalyst electrode was prepared in the same procedure mentioned above. All electrochemical tests, including linear sweep voltammetry (LSV) and chronoamperometry, were performed at room temperature in 0.1 M KOH solutions, which were purged with O_2 for at least 30 min prior to each measurement. Tests for LSV were scanned between -1.0 and +0.2 V at 10 mV s^{-1}, and LSVs were recorded at various rotating speeds from 400 to 1600 rpm. Chronoamperometry tests were conducted in O_2-saturated 0.1 M KOH at -0.4 V with a rotation rate of 900 rpm.

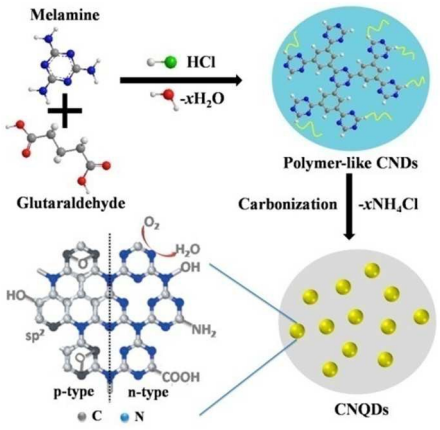

Fig. 1 Schematic illustration of the formation of CNQDs by a facile one-pot hydrothermal treatment.

Results and Discussion

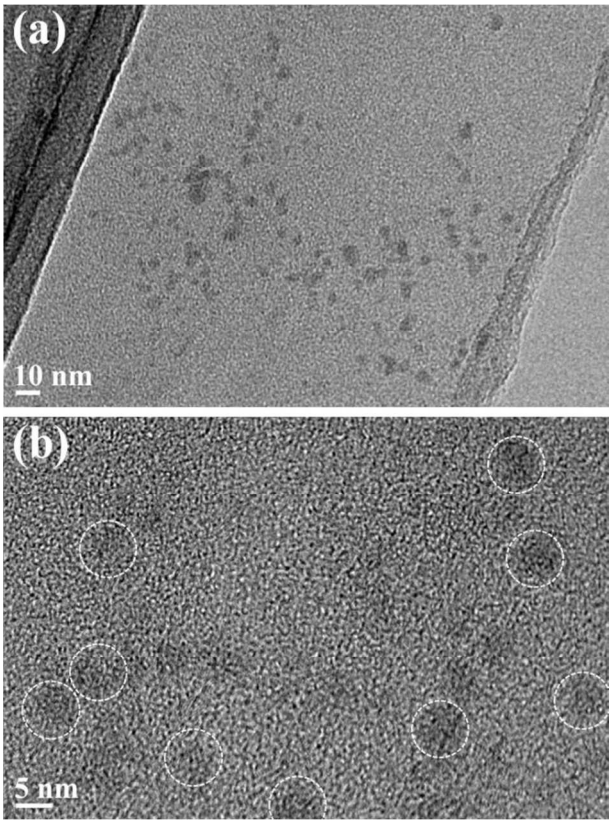

Fig. 2 (a) TEM image of CNQDs. (b) HRTEM image of CNQDs.

In this work, we describe one-pot hydrothermal synthetic carbonization method for the novel preparation of carbon-nitrogen quantum dots (CNQDs). The fabrication process of CNQDs using melamine and glutaraldehyde as precursors is illustrated in Fig. 1, and further details of the synthesis can be found in the Experimental section. In order to estimate the products after the hydrothermal treatment, X-ray diffraction pattern of the prepared dry samples without any treatment is shown in Fig. S1. The well-defined peaks at 2θ values of 22.8°, 32.5°, 40.2°, 46.7°, 52.7°, and 58.2° are in good agreement with the Joint Committee on Powder Diffraction Standards (JCPDS) card 34-0710, which confirms the formation of NH_4Cl in our speculation. The relatively sharp diffraction peaks at around 2θ = 27.4° and 45.4°, which is corresponding to the (002) and (101) diffractions of g-C_3N_4, indicating the partially graphitized-like structure of CNQDs (Fig. S1).[11] To further confirm the compositions, the products were subjected to TGA/DSC thermogravimetric analysis between the temperatures from room temperature to 800 °C in N_2. From the previous analyses, it is noted that the products may consist of NH_4Cl and CNQDs. A series of discrete mass-loss events are observed corresponding to the compositions from the XRD. Residual small molecules are removed by extending treatment from room temperature to 250 °C. Heating to 350 °C, a major endothermic peak occurs due to the decomposition of NH_4Cl (T_{sub}=340 °C), and the sample lost about 30 % of its mass. Further treatment to 400 °C and final 800 °C produced an additional loss equal to 34 %, which is attributed

to the decomposition and condensation of g-C_3N_4,[12] leaving 26 % of the initial mass behind (presumably carbon, Fig. S2). Fig. 2a shows the transmission electron microscope (TEM) image of as-prepared CNQDs. The collected CNQDs are monodispersed with a uniform diameter of ca. 3~8 nm in Fig. 2b and Fig. S3 (5.3 nm average diameter, similar to the reported).[13] To investigate their morphologies, the suspensions of CNQDs were transferred to the surfaces of freshly exfoliated mica and characterized by atom force microscopy (AFM). It is found that CNQDs consist mainly of disordered particles (Fig. S4). For CNQDs, nanodots of about 6 nm diameter and 4-5 nm thickness are found, which is similar to the TEM images.

X-ray photoelectron spectroscopy (XPS) measurements were performed to determine the composition of the as-prepared CNQDs. The XPS survey spectrum of the resultant CNQDs after dialysis (Fig. 3a) shows a predominant C 1s peak at ca. 284.6 eV, a pronounced N 1s peak at ca. 400 eV, an O 1s peak at ca. 532 eV and Cl 2p peak at ca. 200 eV. The C 1s spectrum (Fig 3b) shows four peaks at 284.6, 286.0, 286.6, and 288.1 eV, which are attributed to C–C, C–N, C–O, and C=N/C=O, respectively, indicating the existence of carbon atoms connected to N and O heteroatoms. The N 1s spectrum (Fig. 3c) shows three peaks at 399.5, 400.5, and 401.5 eV, which are attributed to the C–N–C (pyridine N), N–$(C)_3$ (pyrrolic N), and N–H bands, respectively.[13] The O/C atomic ratio for CNQDs is ca. 13 %, similar to graphene (ca. 15 %).[14] The N/C atomic ratio is calculated to be 20.7 %, which is higher than the N-doped carbon materials and lower than g-C_3N_4 (N/C atomic ratio 4/3) reported previously.[1] Some previous works have reported that a good N incorporation (both pyridine N & pyrrolic N) is considered to be excellent electronic conductivity, and good catalytic activity toward the ORR.[15] Moreover, the O 1s spectrum (Fig. 3d) shows the only signal peak at 531.6 eV corresponding to carbonyls, which is in accordance with the characteristic carbon state of C=O in the C 1s spectrum. And these results are consistent with the corresponding FTIR spectra (Fig. S5). Peaks at around 3402, 3216 and 2934 cm^{-1} correspond to the OH, NH and C=C-H stretching modes, respectively. Note the C=O stretch is at 1735 cm^{-1}, and bands at 1660 and 1536 cm^{-1}, 1450 cm^{-1} can be attributed to the C=N and C=C stretching mode of the polycyclic aromatic hydrocarbons, whereas others at 1165 and 1078 cm^{-1} correspond to the asymmetric stretching vibrations of C-NH-C. These results reveal that the molecular structures of CNQDs mainly contain polycyclic aromatic and aromatic CN groups.[6] And chemical and structural information about CNQDs was further obtained from the solid-state ^{13}C NMR spectrum (Fig. S6), signals in the range of 30-45 ppm are corresponding to aliphatic (sp^3) carbon atoms, and signals from 100-185 ppm are indicative of sp^2 carbon atoms.[16] Therefore, we can conclude that the as-prepared CNQDs are mainly composed of polycyclic aromatic and aromatic CN species derived from the polymerization and carbonization of melamine and glutaraldehyde, as well as possessing abundant amino, and carbonyl/carboxylate groups on their surface. The possible chemical reactions are shown in Fig. S7.

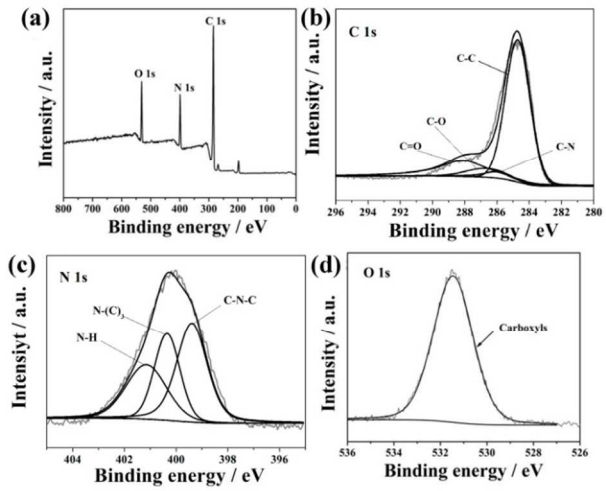

Fig. 3 (a) XPS spectra of CNQDs. High-resolution (b) C 1S, (c) N 1S and (d) O 1S spectra.

Fig. 4a shows the optical properties of CNQDs. The absorption spectrum shows a weak absorption feature at ca. 282 nm, which is a typical characteristic of fluorescent CQDs.[17] The normal and normalized PL spectra of CNQDs displays an excitation-dependent PL behavior. When the excitation wavelength is changed from 360 to 460 nm, the PL peaks shifted from 440 (black) to 512 nm (yellow). The bright and colorful PL may be attributed to the synergistic effect of the carbonitride core and the surface/molecular state of the CNQDs.[18] The photographs also show the CNQDs aqueous solution has a brighter blue fluorescence under 365 nm UV light (Inset of Fig. 4b). By selecting quinine sulfate in water as the standard and 360 nm as the excitation wavelength, the QYs of the CNQDs was measured and calculated to be 31 % (Table S1), which is higher than the previously reported CQDs. This may be caused by the high surface passivation by various amine groups (perhaps owing to amide-containing fluorophores), as the already reported.[5] Even after being kept for 1 year in air at room temperature, the CNQDs still exhibited the stable fluorescence properties (Fig. S8), which offers another advantage for their future applications. The photoluminescent excitation (PLE) spectrum recorded with the strongest luminescence shows only a sharp peak at 365 nm (Fig. 4b). Thus, we speculate that the σ orbital of CNQDs is more stable, and the excited electrons are more easier transition back to the σ orbital.[19] Similar to our previously reported, we also conducted further studies on the upconversion performance. Unfortunately, the upconverted emissions peaks did not occur when the excitation wavelength changed from 600 to 700 nm with the same optical testing conditions. It is concluded that the upconverted fluorescent is the inherent characteristic of our preparation GQDs.[20]

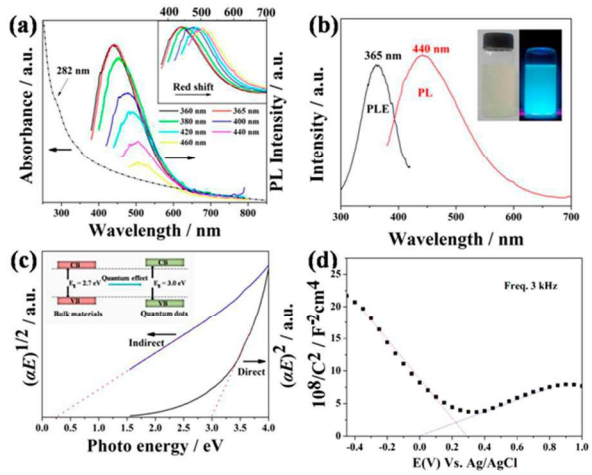

Fig. 4 (a) UV-vis absorption (Abs) and photoluminescent (PL) spectra of the CNQDs at different excitation wavelengths. Inset: the corresponding normalized PL spectra. (b) PLE spectrum with the detection wavelength of 440 nm and PL spectrum excited at 365 nm. Inset: Photograph of CNQDs aqueous solution taken under visible and UV light. (c) Plots of $(\alpha E)^2$ and $(\alpha E)^{1/2}$ against photon energy (E) for CNQDs solution, where α is the absorbance. Inset: schematic energy level diagrams of bulk g-C_3N_4 and CNQDs. (d) Variation of capacitance (C) with the applied potential in 2 M H_2SO_4 presented in the Mott-Schottky relationship for CNQDs electrode. The capacitance was determined by electrochemical impedance spectroscopy.

We plotted the square and square root of the absorption energy (αE, where α is the absorbance) against the photon energy (E) to determine the energies of the direct and indirect gaps, respectively. The converted plots (Fig. 4c) do not show a sharp absorption edge for specific gap energy. This occurs because the CNQDs consist of g-C_3N_4 quantum dots with various oxidation and nitridation levels. Particle size variation also contributed to the broadening of the absorption edge. Applying an approximate linear extrapolation, an apparent energy of 3.0 eV for direct transition and 0.25 eV for indirect transition are obtained for the CNQDs (Fig. 4c). And due to the quantum effect, the energy gap of CNQDs is wider than the bulk g-C_3N_4 materials (2.7 eV).[21] The electrochemical impedance spectroscopic analyses were conducted and the Mott-Schottky equation was used to identify the type of conductivity of the CNQDs.[22] Fig. 4d shows the capacitance values of the space charge region obtained at various applied potentials. According to the Mott-Schottky equation, a linear relationship of $1/C^2$ versus applied potential can be obtained. Fig. 4d shows straight lines with negative and positive slopes located in different potential regimes. The Mott-Schottky plots at different frequency (3, 5, 7 and 9 kHz) are also displayed in Fig. S9. The negative and positive slopes correspond to p- and n-type conductivities, respectively. The results indicate the co-existence of both p- and n-type conductivities in CNQDs.[10] The high doped nitrogen and oxygen introduction process successfully created n- and p-type domains in CNQDs (Fig. 1), which was consistent with the XPS spectra of CNQDs. In addition, the stronger PL emission from the CNQDs might be associated with the formation of p-n type photochemical diodes. The electron-hole recombination generally results from electronic transition among the sp2 clusters and the boundary of oxidized regions; that is, the recombination occurs in the vicinity of the sp2 clusters. The small sp2 clusters may serve as the interfacial junction between the p- and n-type domains distributed in the CNQDs.

Li et al. used p-type Cu_2O semiconductor as photocathode in solar-driven microbial photoelectrochemical cell due to its favorable band structures and the existence of oxygen vacancies.[23] So CNQDs with co-existence of p- and n-type conductivities can be applied in photocathode. In addition, N-doped carbon nanomaterials such as N-CNTs and N-graphene have been demonstrated to hold promise as metal free electrocatalysts to replace the commercially available Pt-based catalysts for the ORR.[24] Apart from their unique luminescence properties, CNQDs are also expected to possess electrocatalytic activity for the ORR. As evidenced by the XPS analysis, it has been demonstrated that both pyridinic N and pyrrolic N exist in the CNQDs, which are supposed to be favorable for enhancing the ORR activity.[25] However, the extremely low electrical conductivity of CNQDs affected the ORR electrocatalytic activity. So the catalysts were prepared by chemical coupling the CNQDs on the Ag NPs (CNQDs/Ag NPs) (Fig. S10), which was not only to increase the conductivity, but also enhanced the photoelectric effect of CNQDs. Ag NPs exhibit unique, improved electronic and optical properties. The impedance Nyquist plots spectra of CNQDs/Ag NPs are displayed in Fig. S11. It is well established that the introduction of Ag NPs yields an electronic wire on the electrode, resulting in a low electron transfer resistance (ca. 25 Ω). As compared to CNQDs, the interfacial electron transfer resistance of CNQDs/Ag NPs correspondingly decreased from ca. 370 Ω to 140 Ω. The results indicate that the chemical coupling Ag NPs dramatically improved the ability of electronic transfer.

Linear-sweep voltammograms (LSVs) tests were first carried out in O_2-saturated 0.1 M KOH by using a rotating disk electrode (RDE) to investigate the electrocatalytic activity and kinetics of CNQDs and CNQDs/Ag NPs catalysts. LSVs for Ag NPs, CNQDs, CNQDs/Ag NPs and the commercial Pt/C at 1600 rpm are shown in Fig. 5a. The limiting current density and onset potential are two important criterion to evaluate the ORR activity of catalysts. The CNQDs/Ag NPs presents a positive onset potential of -0.081 V and a current density of 4.09 mA cm^{-2} at -0.5 V, very close to those of Pt/C (-0.022 V and 4.99 mA cm^{-2}), and much higher than those of Ag NPs (-0.261 V and 2.07 mA cm^{-2}), and CNQDs (-0.169 V and 2.69 mA cm^{-2}). The more positive onset potential and larger current density of CNQDs/Ag NPs than those of Ag NPs, and CNQDs should also suggest the existence of a synergetic effect between CNQDs and Ag NPs in the composite. Apparently, in both limiting current density and onset potential, CNQDs/Ag NPs catalyst is significantly superior to the individual CNQD, and even close to the performance of the commercial Pt/C catalyst, indicating the important role of the chemical coupling Ag NPs.

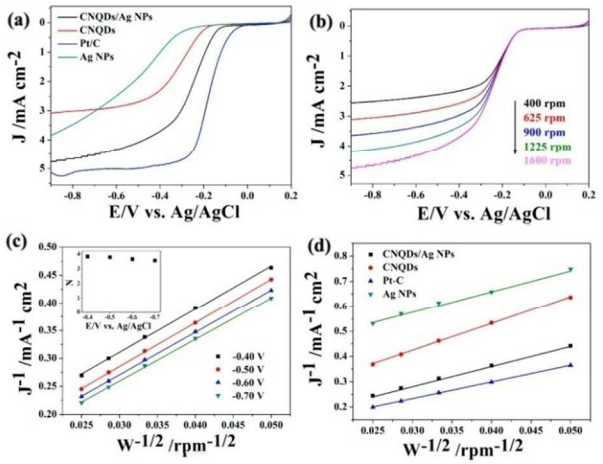

Fig. 5 (a) LSVs for CNQDs, CNQDs/Ag NPs Pt/C and Ag NPs in O_2-saturated 0.1 M KOH at a rotating speed of 1600 rpm. (b) LSVs for CNQDs/Ag NPs at different rotating speeds. (c) K-L plots and the corresponding electron transfer numbers of CNQDs/Ag NPs. (d) K-L plots for different samples at -0.50 V.

LSV curves at different electrode rotation rates for CNQDs/Ag NPs are shown in Fig. 5b. The K-L plots are obtained by linear fitting of the inverse square root of rotating speed *vs* reciprocal current density at rotation rate from 400 to 1600 rpm. The measured current density shows the typical increase with increasing rotation rate due to the enhanced diffusion of O_2 molecules in the electrolyte.[7] Fig. 5c shows the corresponding Koutecky–Levich plots (J^{-1} *vs.* $W^{-1/2}$) at different potentials for CNQDs/Ag NPs, the transferred electron number per O_2 molecule involved in the ORR process was determined based on the Koutecky−Levich equations (eq. 1, 2 in the SI).[26,27] The parallel and straight fitting lines imply first-order reaction kinetics with respect to the dissolved oxygen. The transferred electron number (n) value for CNQDs/Ag NPs was derived to be 3.3-3.8 over the potential range from -0.40 to -0.70 V (the inset of Fig. 5c), suggesting a four-electron dominated process for ORR on the CNQDs/Ag NPs electrodes.[21] The Ag NPs showed a smaller value of n = 1.38 (-0.5 V, inset Fig. S12f), indicative of two electron transfer pathways during the ORR reaction. The corresponding K-L plots of all materials prepared reveal that a good linear (Fig. 5d) and the electrons transferred number of the CNQDs and CNQDs/Ag NPs were 2.3 and 3.7 (-0.5 V, inset Fig. S12b, inset Fig. 5c), respectively, indicating a nearly two-electron pathway for CNQDs and a nearly four-electron pathway for CNQDs/Ag NPs. These results indicate that the well-designed CNQDs/Ag NPs is a promising electrocatalyst for the ORR under alkaline conditions. The polarization curve of Pt/C and corresponding K-L plots are also obtained under the same experimental condition (Fig. S12c). The electrons transferred number of Pt/C in our study was close to 4 (inset Fig. S12d). The higher electron transfer number and J_k of CNQDs/Ag NPs than those of Ag NPs and CNQDs further manifest the synergetic promotion of ORR performance from the chemical coupling CNQDs on the Ag NPs. Additionally, chronoamperometric durability tests for the ORR were also performed (Fig. S13). The Pt/C catalyst shows a 16.8 % decrease in activity after 10000 s at -0.4 V. As a comparison, CNQDs/Ag NPs retains a high relative current of 89.3 % after 10000 s, indicating a superior stability of the active reaction sites on CNQDs/Ag NPs than on commercial Pt/C in an alkaline environment. So duo to the co-existence of both n- and p-type conductivities and excellent catalytic activity for ORR, the CNQDs may be a good potential photocathode material for fuel cells and solar cells in the future. In addition, the superior luminescence characteristic of CNQDs allows them to be used for biomedical imaging and other optoelectronic applications.

Conclusions

We have developed a simple route to synthesize CNQDs with a uniform size of ca. 5 nm on a large scale through hydrothermal treatment of melamine and glutaraldehyde. Optical property characterization indicates CNQDs display excellent PL properties, with a high QYs of ca. 31 %. Moreover, due to the N-doped carbon dots and synergistic effect of Ag NPs, the resulted CNQDs/Ag NPs composite catalyst shows a high catalytic activity and superior stability to the commercial Pt/C catalyst for the ORR. Apart from the use of CNQDs as a catalyst for ORR, their unique luminescence properties indicate a promising potential for bioimaging and light-emitting diodes, among many other potential applications.

Acknowledgements

This work was supported by the National Natural Science Foundation of China (21136006, 21206043, 21236003, 21322607, 21406072), the Shangai Shuguang Scholars Program (13SG31), the Shanghai Rising-Star Program (13QA1401100), Program for Professor of Special Appointment (Eastern Scholar) at Shanghai Institutions of Higher Learning, Project funded by China Postdoctoral Science Foundation (2014M560307, 2014M561497), and the Fundamental Research Funds for the Central Universities.

Notes and references

[a] *Key Laboratory for Ultrafine Materials of Ministry of Education, School of Materials Science and Engineering, East China University of Science and Technology, Shanghai 200237, China. Fax: +86-21-64250624; E-mail: czli@ecust.edu.cn (C. Li)*

b *Shanghai Nanotechnology Promotion Center, Shanghai 200237, China*

† Electronic Supplementary Information (ESI) available: Experimental Section, Fig. S1-S13. See DOI: 10.1039/b000000x/

1. W. Li, Z. Zhang, B. Kong, S. Feng, J. Wang, L. Wang, J. Yang, F. Zhang, P. Wu, D. Zhao, *Angew. Chem. Int. Ed,* 2013, **31**, 8151-8155.
2. J. Shen, Y. Zhu, X. Yang, C. Li, *Chem. Commun.,* 2012, **48**, 3686-3699.
3. S. N. Barer, G. A. Baker, *Angew. Chem. Int. Ed.*, 2010, **38**, 6726-6744.
4. B. Kong, A. Zhu, C. Ding, X. Zhao, B. Li, Y. Tian, *Adv. Mater,* 2012, **24**, 5844-5848.
5. S. Zhu, Q. Meng, L. Wang, J. Zhang, Y. Song, H. Jin, K. Zhang, H. Sun, H. Wang, B. Yang, *Angew. Chem. Int. Ed,* 2013, **52**, 3953-3957.
6. S. Liu, J. Tian, L. Wang, Y. Zhang, X. Qin, Y. Luo, A. M. Asiri, A. O. Al-Youbi, X. Sun, *Adv. Mater,* 2012, **24**, 2037-2041.

7. K. Gong, F. Du, Z. Xia, M. Durstock, L. Dai, *Science*, 2009, **323**, 760-764.
8. S. Wang, D. Yu, L. Dai, *J. Am. Chem. Soc,* 2011, **133**, 5182-5185.
9. Y. Li, Z. Zhou, P. Shen, Z. Chen, *ACS Nano,* 2009, **3**, 1952-1958.
10. T. Yeh, C. Teng, S. Chen, H. Teng, *Adv. Mater,* **2014**, 20, 3297-3303.
11. Y. Zhang, Q. Pan, G. Chai, M. Liang, G. Dong, Q. Zhang, J. Qiu, *Sci. Rep,* 2013, **3**, 1943.
12. J. Xu, Y. Li, S. Peng, G. Lu, S. Li, Phys. *Chem. Chem. Phys,* 2013, **15**, 7657-7665.
13. Y. Li, Y. Zhao, H. Cheng, Y. Hu, G. Shi, L. Dai, L. Qu, *J. Am. Chem. Soc,* 2012, **134**, 15-18.
14. L. Qu, Y. Liu, J. B. Baek, L. Dai, *ACS Nano,* 2010, **4**, 1321-1326.
15. W. Ding, Z. Wei, S. Chen, X. Qi, T. Yang, J. Hu, D. Wang, L. Wan, S. F. Alvi, L. Li, *Angew. Chem. Int. Ed*, 2013, **45**, 11755-11759.
16. W. Cai, R. D. Piner, F. J. Stadermann, S. Park, M. A. Shaibat, Y. Ishii, D. Yang, A. Velamakanni, S. J. An, M. Stoller, J. An, D. Chen, R. S. Ruoff, *Science,* 2008, **321**, 1815-1817.
17. C. Zhu, J. Zhai, S. Dong, *Chem. Commun,* 2012, **48**, 9367-9369.
18. J. Wang, C. F. Wang, S. Chen, *Angew. Chem. Int. Ed*, 2012, **51**, 9297-9301.
19. D. Pan, J. Zhang, Z. Li, M. Wu, *Adv. Mater,* 2010, **22**, 734-738.
20. J. Shen, Y. Zhu, C. Chen, X. Yang, C. Li, *Chem. Commun,* 2011, **47**, 2580-2582.
21. Y. Zheng, J. Liu, J. Liang, M. Jaroniec, S. Z. Qiao, *Energy Environ. Sci,* 2012, **5**, 6717-6731.
22. J. N. Nian, C. C. Tsai, P. C. Lin, H. Teng. *J. Electrochem. Soc,* 2009, **156**, H567-H573.
23. F. Qian, G. Wang, Y. Li, *Nano Lett,* 2010, **10**, 4686-4691.
24. X. Yang, W. Zou, Y. Su, Y. Zhu, H. Jiang, J. Shen, C. Li, *J. Power Sources,* 2014, **266**, 36-42.
25. Y. Su, H. Jiang, Y. Zhu, X. Yang, J. Shen, W. Zou, J. Chen, C. Li, *J. Mater. Chem. A*, 2014, **2**, 7281-7287.
26. R. Ning, C. Ge, Q. Liu, J. Tian, A. M. Asiri, K. A. Alamry, C. Li, X. Sun. *Carbon*, 2014, **78**, 60-69.
27. R. Ning, J. Tian, A. M. Asiri, A. H. Qusti, A. O. Al-Youbi, X. Sun. *Langmuir*, 2013, **29**, 13146-13151.